

Article

# Electromagnetic Actuator System Using Witty Control System

Der-Fa Chen, Shen-Pao-Chi Chiu, An-Bang Cheng and Jung-Chu Ting \*

Department of Industrial Education and Technology, National Changhua University of Education, Changhua 500, Taiwan; dfchen@cc.ncue.edu.tw (D.-F.C.); baochy@ms47.hinet.net (S.-P.-C.C.); jhenganbang@gmail.com (A.-B.C.)

\* Correspondence: d0331019@gm.ncue.edu.tw; Tel.: +886-4-723-2105

**Abstract:** Electromagnetic actuator systems composed of an induction servo motor (ISM) drive system and a rice milling machine system have widely been used in agricultural applications. In order to achieve a finer control performance, a witty control system using a revised recurrent Jacobi polynomial neural network (RRJPNN) control and two remunerated controls with an altered bat search algorithm (ABSA) method is proposed to control electromagnetic actuator systems. The witty control system with finer learning capability can fulfill the RRJPNN control, which involves an attunement law, two remunerated controls, which have two evaluation laws, and a dominator control. Based on the Lyapunov stability principle, the attunement law in the RRJPNN control and two evaluation laws in the two remunerated controls are derived. Moreover, the ABSA method can acquire the adjustable learning rates to quicken convergence of weights. Finally, the proposed control method exhibits a finer control performance that is confirmed by experimental results.

**Keywords:** bat search algorithm; Jacobi polynomial neural network; Lyapunov stability principle; three-phase induction servo motor; rice milling machine system



**Citation:** Chen, D.-F.; Chiu, S.-P.-C.; Cheng, A.-B.; Ting, J.-C. Electromagnetic Actuator System Using Witty Control System. *Actuators* **2021**, *10*, 65. <https://doi.org/10.3390/act10030065>

Academic Editor: Oscar Barambones

Received: 1 March 2021

Accepted: 19 March 2021

Published: 22 March 2021

**Publisher's Note:** MDPI stays neutral with regard to jurisdictional claims in published maps and institutional affiliations.



**Copyright:** © 2021 by the authors. Licensee MDPI, Basel, Switzerland. This article is an open access article distributed under the terms and conditions of the Creative Commons Attribution (CC BY) license (<https://creativecommons.org/licenses/by/4.0/>).

## 1. Introduction

Compared to other three-phase motors, three-phase induction motors (IMs) are widely used in many industrial and commerce applications due to their simple structures and easy maintenance. In order to achieve better control performance, IMs have served as induction servo motors (ISMs) via structural improvement and encoder installation. Therefore, ISMs have been broadly applied to various servo fields such as computer numerical control (CNC) machine tools and milling machines [1–4]. Li et al. [1] proposed a new intelligent adaptive CNC system design for a milling machine by using the neural network controller to achieve better control characteristics. Huang et al. [2] proposed an approach for cutting the force control of CNC machines. This approach with a state estimator was executed by using the observed variables and cutting force to achieve robust control. Recently, the developed approach was applied to a milling machine center. Gomes and Sousa [3] proposed the adaptive control of milling machine cutting force by using an artificial neural network to obtain good results. Mikolajczyk [4] proposed a system of a numerical control conventional milling machine with electromagnetic clutches by using VB6 special software to control the machine with G-code. However, these control systems took a long time to fulfill nonlinear disturbances so that they resulted in lower calculation efficiency. Thereby, the aim of the proposed witty control system using a revised recurrent Jacobi polynomial neural network (RRJPNN) control and two remunerated controls with altered bat search algorithm (ABSA) and progressive weight pruning approaches for the ISM driving the rice milling machine is to reduce computing time and to quicken convergence of weights. Meanwhile, the proposed witty control system can increase machining efficiency and control characteristics.

Due to their good learning capability, many neural networks (NNs) have been applied in many linear and nonlinear systems, such as optimal hysteresis modelling methods

of magnetic controlled shape memory alloys (MSMAs) [5], control of ionic electroactive polymer actuators [6], predicting the driving force for a multicyclic driving experiment of silicone/ethanol soft composite material actuators [7], and design of a 2-DOF ankle exoskeleton with a bidirectional tendon-driving actuator and a polycentric structure [8]. These NNs take a long time to conduct training and learning of a system. In order to reduce calculating time, some polynomial function NNs have been proposed for applications in function approximation [9], dynamic control for continuously variable transmission [10], approximation and estimation of nonlinear functions [11] and backstepping control of synchronous reluctance motor (SynRM) drive systems [12]. As heuristic comprehension methods were applied to adjust learning rates of weights, these NNs that were applied in control systems resulted in slower convergence. Thereby, the proposed NN that is combined with Jacobi polynomials [13] is a novel NN structure that has not yet been applied to estimate, predict and control nonlinear systems. The feedforward Jacobi polynomial neural network (FJPNN) [14] may not effectively approximate nonlinear dynamics because there is no recurrent path. Therefore, many recurrent NNs have been applied in nonlinear system identification [15], model predictive control for continuous pharmaceutical manufacturing [16], estimation in the effective connectivity of electroencephalography [17] and visual field prediction [18] because of higher accuracy and better identification. Due to it having more advantages than the feedforward FJPNN, the RRJPNN control by adopting the ABSA method with progressive weight pruning approach has not yet been used to control the ISM driving the rice milling machine system in order to cut down computation complexity.

The customary optimization algorithm is applied when solving the classic problem of smaller dimensions that are not easily applicable in reality. The swarm intelligence optimization algorithms (SIOAs) were discovered by adopting simulated natural biological systems. Recently, many researchers have proposed the SIOAs, such as bat algorithm (BA) [19], particle swarm optimization (PSO) [20], social learning optimization algorithm (SLOA) [21], chicken swarm optimization algorithm (CSOA) [22] and ant colony algorithm (ACO) [23]. Yang [24] first proposed the bat algorithm (BA), which is based on the swarm intelligence heuristic search algorithm. Due to it having fewer parameters, powerful robustness, and a simple and easy implementation, BA has attracted more and more attention in the search for a global optimal solution. The BA has been applied in multiobjective function optimizations with a neural network model [19], economic operations [25] and numerical optimizations [26]. However, the local search method by adopting BA has the shortcoming of precocious convergence and does not perform well in the early search stage. Therefore, the proposed altered bat search algorithm (ABSA) method is a novel method to avoid precocious convergence. Moreover, a progressive weight pruning approach based on the ABSA method is proposed to deal with nonconvex optimization problems. The ABSA method with modified loudness and modified pulse rate is used to adjust two optimal learning rates. Thereby, a novel fast-convergence algorithm applied to RRJPNN with two learning rates by adopting the ABSA method with the progressive weight pruning approach that is used to adjust two optimal learning rates and to quicken convergence of weights is proposed in this paper. At last, some tested results show that the fine control performances are confirmed by the proposed control method.

The organization of this research is as follows. Section 2 introduces some explanations of the ISM driving the rice milling machine system. Section 3 advocates the witty control system by adopting the RRJPNN control and two remunerated controls with ABSA. Section 4 promotes the tests and experimental results for the ISM driving the rice milling machine system. Section 5 presents the discussions and explanations of some experimental results. Section 6 describes some conclusions.

## 2. Materials

The complete system consists of three subparts that are: the ISM and drive system, the digital signal processor (DSP) control system and the rice milling machine system, as below.

### 2.1. System Description

The ISM and drive system consist of a mounted encoder three-phase ISM with a rotor that adopts a high moment of inertia and low frictional coefficient, a rectifier, an LC filter, an isolated circuit, a lockout-time circuit, a current sensing circuit, an analog-digital conversion, and the voltage fed converter with 3-leg 6-switch transistor power devices. The DSP control system is composed of a speed control, a proportional-integral (PI) current control and an indirect field-oriented control (IFOC) [27–29]. The IFOC consists of a space-vector pulse-width-modulation control,  $\sin \theta_t / \cos \theta_t$  creation, a coordinate transformation and an inverse coordinate transformation. The rice milling machine system is composed of a feed chopper, milling room, main idler, idler 1, idler 2, chaff suction fan, jet fan, chaff outlet, inlet chopper mouth, rice outlet, thickness adjustment lever, belt 1 and belt 2. The arrangement of the ISM driving the rice milling machine system is shown in Figure 1.

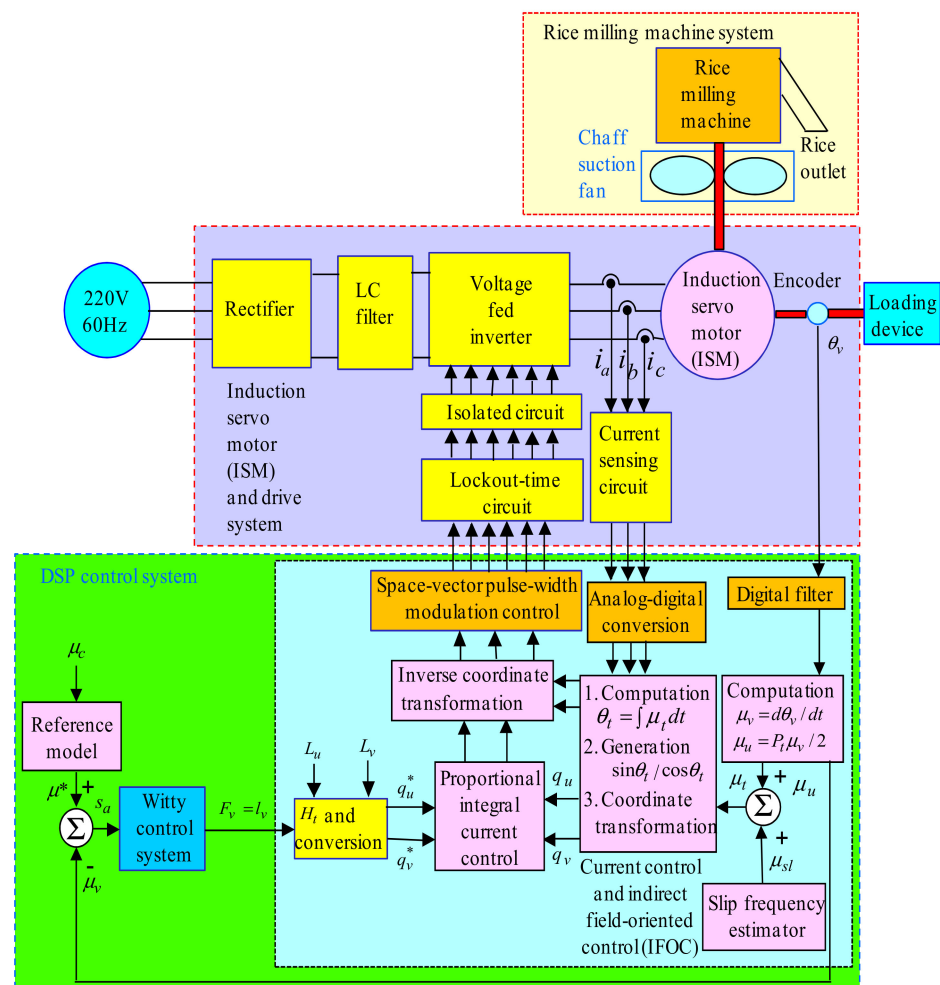


Figure 1. Arrangement of the induction servo motor (ISM) driving the rice milling machine system.

### 2.2. System Model

The voltage equations in the three-phase ISM by using the simplified coordinate frame transforms, from  $a-b-c$  to  $u-v$ , and the Clarke and Park transformations by using the IFOC [27–29] can be represented by

$$w_u = r_a q_u - \mu_t (L_v q_v + L_{uv} q_u) + \frac{d(L_u q_u + L_{uv} q_v)}{dt} \tag{1}$$

$$w_v = r_a q_v + \mu_t (L_u q_u + L_{uv} q_v) + \frac{d(L_v q_v + L_{uv} q_u)}{dt} \tag{2}$$

$$0 = r_b q_{ur} + (\mu_t - \mu_u)(L_u q_{ur} + L_{uv} q_{vr}) + \frac{d(L_v q_{vr} + L_{uv} q_{ur})}{dt} \tag{3}$$

$$0 = r_b q_{vr} + (\mu_t - \mu_u)(L_v q_{vr} + L_{uv} q_{ur}) + \frac{d(L_u q_{ur} + L_{uv} q_{vr})}{dt} \tag{4}$$

where  $w_u$  and  $w_v$  are the  $u - v$  axis stator voltages.  $q_u$  and  $q_v$  are the  $u - v$  axis stator currents.  $q_{ur}$  and  $q_{vr}$  are the  $u - v$  axis rotor currents.  $L_u, L_v$  and  $L_{uv}$  are the  $u - v$  axis self-inductances and mutual inductance, respectively.  $r_a$  and  $r_b$  are the stator and equalized rotor resistances.  $\mu_v$  and  $\mu_u$  are the mechanical and electrical angular speeds in the ISM.  $\mu_t$  is the electrical angular speed of synchronous flux [27]. The electromagnetic torque  $F_a$  [28,29] in the ISM can be described as

$$F_v = \frac{3P_t[\varphi_v q_u - \varphi_u q_v]}{4} = \frac{3P_t[L_v q_v q_u - L_u q_u q_v]}{4} = \frac{3P_t[L_v - L_u]}{4} q_u q_v \tag{5}$$

where  $\varphi_u$  and  $\varphi_v$  are  $u - v$  axis flux linkages.  $P_t$  is the number of poles.

The ISM driving the rice milling machine system led to a more sluggish performance of the system owing to a nonlinear uncertainty effect. The response of speed control for the ISM driving the rice milling machine system resulted in poor performance. The adumbration view of the ISM and the rice milling machine system is illustrated in Figure 2.

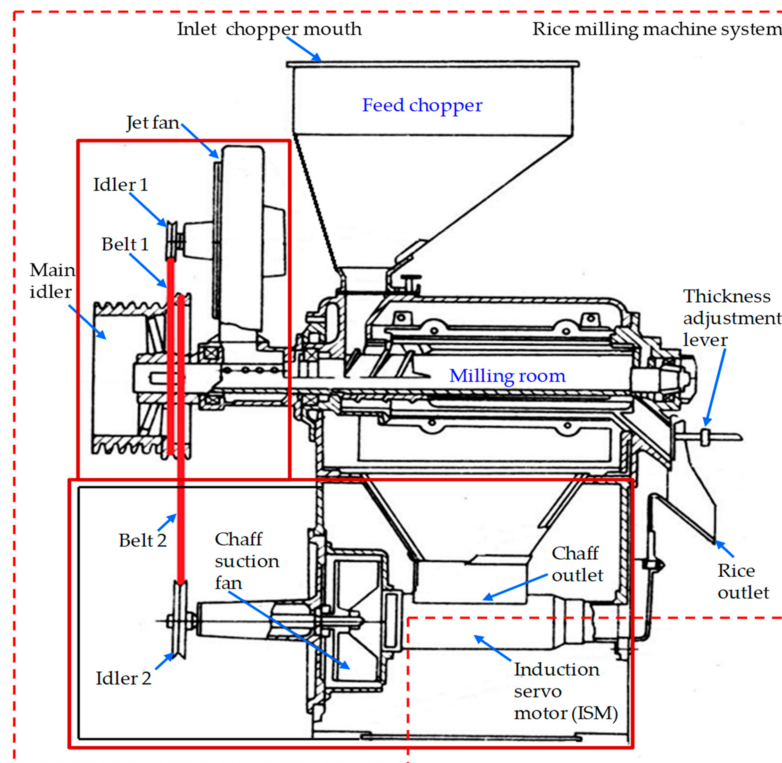


Figure 2. Adumbration view of the ISM and the rice milling machine system.

Considering that the power loss and sliding loss were insignificant, two dynamic equations with simplified kinematics of the rice milling machine system are described as [30–32]:

$$F_v = f_a \frac{d\mu_v}{dt} + g_a \mu_v + \phi_b \mu_b F_d / \mu_v + f_c \frac{d\mu_v}{dt} + g_c \mu_v \tag{6}$$

$$F_d = f_d \frac{d\mu_b}{dt} + g_d \mu_b + f_b \frac{d\mu_b}{dt} + g_b \mu_b + F_b^l (R_{ob}, F_{ob}, F_{vl}, g_b) \tag{7}$$

where  $F_v, F_d$  and  $F_{b1}$  are the electromagnetic torque of the ISM, the output torque of idler 2 and the output torque of the main idler, respectively.  $f_a, f_c, f_d$  and  $f_b$  are the four moments

of inertia in the ISM, in idler 2, in the main idler and in idler 1, respectively.  $g_v, g_c, g_d$  and  $g_b$  are the four viscid frictional coefficients in the ISM, in idler 2, in the main idler and in idler 1, respectively.  $\phi_b$  is the transposition ratios regarding idler 2 and the main idler for the rice milling machine system.  $F_b^l(R_{vb}, F_{vb}, F_{vl}, g_b)$  is the nonlinear coalescence disturbances function including rolling force  $R_{vb}$ , wind force  $F_{vb}$ , and braking force  $F_{vl}$ .  $\mu_v$  and  $\mu_b$  are the speed in idler 2 and the speed in the main idler. Then, the torque equation can be transformed from the main idler to idler 2 by use of a transformed ratio. The modeling of the rice milling machine can be simplified by omitted sliding losses of two belts; thus, the dynamic equation in the ISM driving the rice milling machine system including the coalescence torque from Equations (6) and (7) can be expressed as

$$f_r \frac{d\mu_v}{dt} + g_r \mu_v + (\Delta F_a + F_{b1}) + F_t(F_{1c}, F_{2c}, F_{3c}) = F_v \quad (8)$$

$$F_{b1} = \frac{\phi_b \mu_b [(f_d + f_b) \frac{d\mu_b}{dt} + (g_d + g_b) \mu_b + F_b^l(u_{vb}, F_{vb}, F_{vl}, g_b)]}{\mu_v} \quad (9)$$

$$\Delta F_a = \Delta f_r \frac{d\mu_v}{dt} + \Delta g_r \mu_v \quad (10)$$

where  $g_r = g_a + g_c$  and  $f_r = f_a + f_c$  are the coalescence viscid friction coefficient and the coalescence moment of inertia including the main idler and the ISM.  $\Delta F_a + F_{b1}$  is the huge comprehensive coalescence disturbances and parameter variations.  $F_t(F_{1c}, F_{2c}, F_{3c})$  is the coalescence torque [27] including coulomb friction torque  $F_{3c}$ , Stribeck effect torque  $F_{2c}$  and adding load torque  $F_{1c}$ .  $F_{b1}$  represents the comprehensive coalescence disturbances.  $\Delta F_a$  represents the comprehensive parameter variations.

The DSP control system with current control and IFOC can fulfill a speed control, an IFOC and a proportional-integral (PI) current control. The IFOC consists of a space-vector pulse-width-modulation control,  $\sin \theta_t / \cos \theta_t$ , creation, a coordinate transformation and an inverse coordinate transformation. The control gains of the PI current control are the proportional gain of 19.2 and the integral gain of 8.3 by using the heuristic method [33–35] to obtain a finer dynamic response. The drive system was operated under comprehensive coalescence disturbances and comprehensive parameter variations by adopting the DSP control system in this research.

### 3. Methods

In order to design the control structure, the dynamic equation of Equation (8) is modified as

$$\frac{d\mu_v}{dt} = h_v \mu_v + h_w (\Delta F_a + F_{b1} + F_e) + h_x l_v \quad (11)$$

where  $\Delta F_a + F_{b1} + F_e$  represents the comprehensive coalescence disturbances.  $h_v = -g_r f_r^{-1}$  is a friendly ratio constant and  $|h_v \mu_v| \leq R_v(\mu_v)$  is assumed to be bounded with functional-bounded value  $R_v(\mu_v)$ .  $h_w = -f_r^{-1}$  is a friendly constant concerning the coalescence moment of inertia and  $|h_w F_e| \leq R_b$  is assumed to be bounded.  $h_x = f_r^{-1}$  is a friendly constant concerning the coalescence moment of inertia and  $h_x \leq R_c$  is assumed to be bounded.  $R_b$  and  $R_c$  are two friendly values.  $l_v = F_v$  is the electromagnetic torque of the ISM. The speed difference  $s_a$  is as follows.

$$s_a = \mu^* - \mu_v \quad (12)$$

If the comprehensive coalescence disturbances and the comprehensive parameter variations are favorable and affectionate, the excellent control law can be rewritten by

$$l_v^* = \frac{d\mu^*}{h_x dt} + \frac{c_v s_a}{h_x} - \frac{h_v \mu_v}{h_x} - \frac{h_w (\Delta F_a + F_{b1} + F_e)}{h_x} \quad (13)$$

where  $c_v$  is a positive control gain. Equation (12) and  $l_v^* = l_v$  are substituted into Equation (11), so the error equation can be rewritten by

$$\frac{ds_a}{dt} + c_v s_a = 0 \tag{14}$$

The system will track the wished state value at  $t \rightarrow \infty$  and  $s_a(t) \rightarrow 0$ . Nevertheless, the control system will exhibit a sluggish tracking response under the occurrence of uncertainty. Thereby, the proposed witty control system using an RRJPNN control and two remunerated controls with ABSA shown in Figure 3 were developed to control the ISM driving the rice milling machine system in order to enhance the speed of the tracking response.

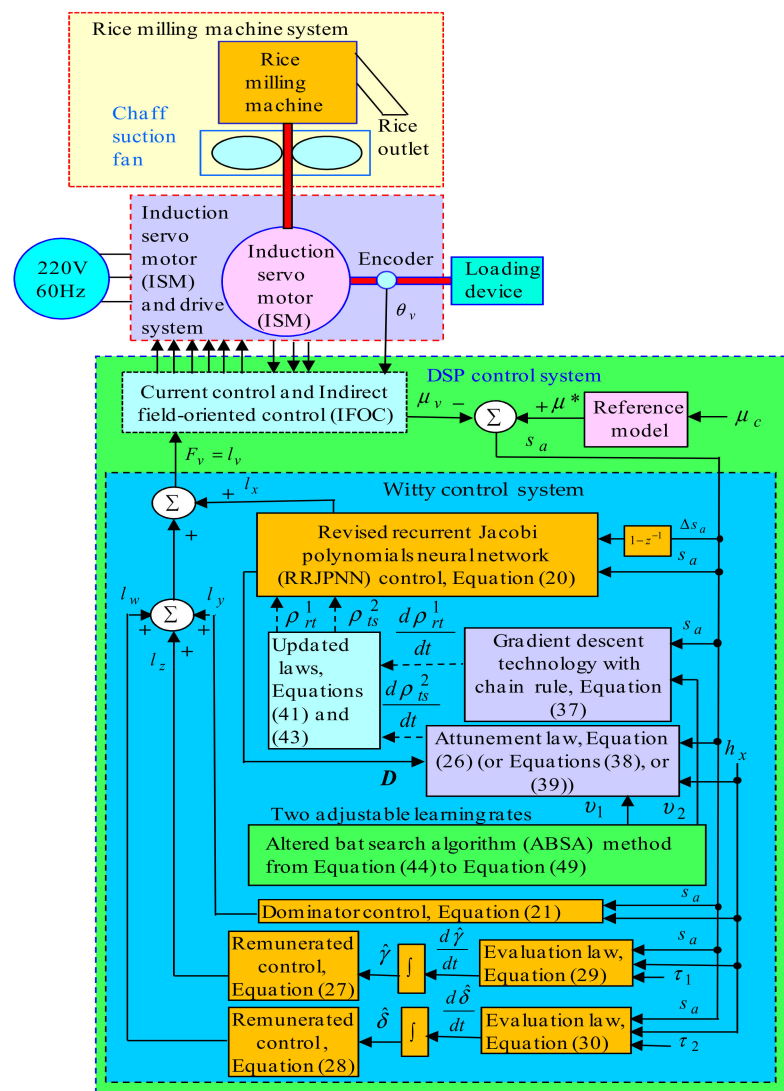


Figure 3. Control frame of witty control system.

The adopted control system is given by

$$l_v = l_x + l_y + l_z + l_w \tag{15}$$

We can use the differential equation of (11), then we can substitute Equations (8) and (12) into this equation. The error equation can be rewritten by

$$\frac{ds_a}{dt} = l_v^* h_x - l_x h_x - l_y h_x - l_z h_x - l_w h_x - c_v s_a \tag{16}$$

where  $l_x$  is the RRJPNN control that acts as the main tracking controller to impersonate the excellent control rule.  $l_y$  is the dominator control that will act in the appropriate region.  $l_z$  and  $l_w$  are two remunerated controls that acts as two remunerated controllers to repay the difference between the excellent control and the RRJPNN control. Then, the three-layer RRJPNN, which is shown in Figure 4, consists of the forehead, center and readward layers. All the informations of all layers are as follows.

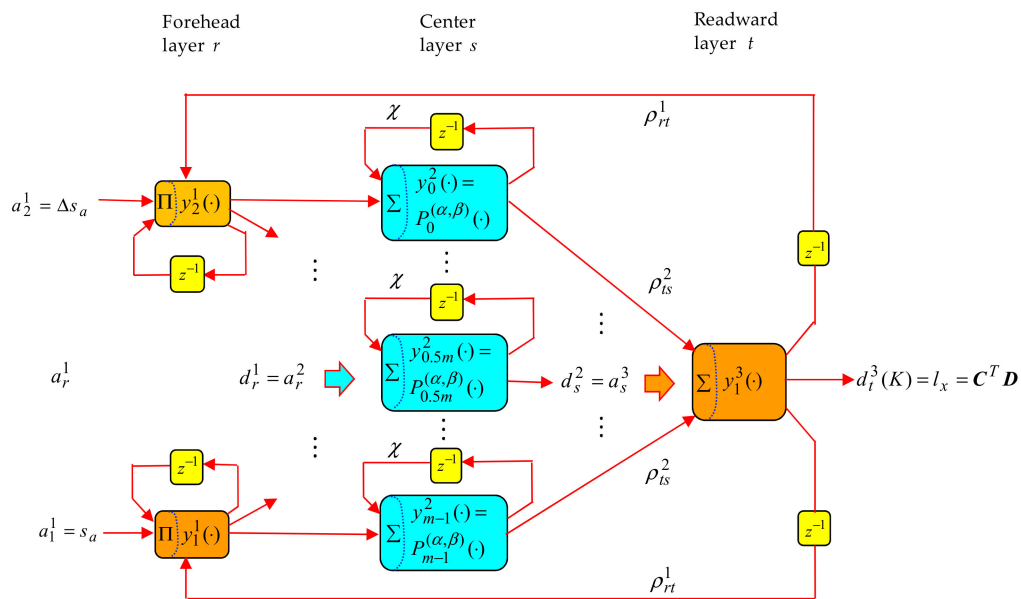


Figure 4. Constitution of the revised recurrent Jacobi polynomial neural network (RRJPNN).

The input and the output informations in the forehead layer are shown below.

$$b_r^1 = \prod_t a_r^1(K) \rho_{rt}^1(K) d_t^3(K-1) d_r^1(K-1), d_r^1(K) = y_r^1(b_r^1) = b_r^1, r = 1, 2 \tag{17}$$

The input and the output informations in the center layer are shown below.

$$b_s^2 = \sum_{r=1}^2 d_r^1(K) + \chi d_s^2(K-1), d_s^2(K) = y_s^2(b_s^2) = P_s^{(\alpha,\beta)}(b_s^2), s = 0, 1, \dots, m-1 \tag{18}$$

The input and the output informations in the readward layer are shown below.

$$b_t^3 = \sum_{s=0}^{m-1} \rho_{ts}^2(K) d_s^2(K), d_t^3(K) = y_t^3(b_t^3) = b_t^3, t = 1 \tag{19}$$

where  $\Pi$  and  $\Sigma$  are the multiplication and summation symbols.  $a_2^1 = s_a(1 - z^{-1}) = \Delta s_a$  and  $a_1^1 = \mu * -\mu_v = s_a$  are the speed difference alteration and the speed difference.  $m$ ,  $\chi$  and  $K$  are the number of nodes of the center layer, the recurrent gain of the center layer and the iteration number, respectively.  $\rho_{rt}^1(K)$  and  $\rho_{ts}^2(K)$  are the recurrent weight between the readward layer and the forehead layer, and the conjoined weight between the center layer and the readward layer.  $y_r^1$ ,  $y_s^2$  and  $y_t^3$  are the three linear activation functions in the forehead, center and readward layers, respectively.  $d_r^1(K)$ ,  $d_s^2(K)$  and  $d_t^3(K)$  are the information of three outputs of nodes in the forehead, center and readward

layers, respectively.  $P_s^{(\alpha,\beta)}(b)$  is the Jacobi polynomial function [13,14] with  $-1 < x < 1$  adopted as the activation function in the center layer—i.e.,  $y_s^2 = P_s^{(\alpha,\beta)}(b)$ .  $P_0^{(\alpha,\beta)}(b) = 1$ ,  $P_1^{(\alpha,\beta)}(b) = (\alpha + 1)(\alpha + \beta + 2)(b - 1)/2$  and  $P_2^{(\alpha,\beta)}(b) = 0.5(\alpha + 1)(\alpha + 2) + 0.5(\alpha + 2)(\alpha + \beta + 3)(b - 1) + 0.125(\alpha + \beta + 3)(\alpha + \beta + 4)(b - 1)^2$  are the 0-, 1- and 2-order Jacobi polynomial functions, respectively. The Jacobi polynomial function with the recurrence relation [13,14] is as below  $(2s + \alpha + \beta - 1)\{(2s + \alpha + \beta)(2s + \alpha + \beta - 2) + \alpha^2 - \beta^2\}P_{s-1}^{(\alpha,\beta)}(b) - 2(s + \alpha - 1)(s + \beta - 1)(2s + \alpha + \beta)P_{s-2}^{(\alpha,\beta)}(b) = 2s(s + \alpha + \beta)(2s + \alpha + \beta - 2)P_s^{(\alpha,\beta)}(b)$ . The output information in the readward layer can be rewritten as  $d_t^3(K) = l_x$ . The RRJPNN control is thus described by

$$d_t^3(K) = l_x = \mathbf{C}^T \mathbf{D} \tag{20}$$

where  $\mathbf{D} = [d_0^2 \ \dots \ d_{m-1}^2]^T$  and  $\mathbf{C} = [\rho_{10}^2 \ \dots \ \rho_{1,m-1}^2]^T$  are the input information and weight vectors in the readward layer.

The dominator control  $l_y$  can be represented by

$$l_y = \frac{1}{h_x} \left[ \left| \frac{d\mu_v}{dt} \right| + |c_v s_a| + R_v(\mu_v) + R_b \right] \text{sgn}(s_a h_x) \tag{21}$$

The dominator control will act in the appropriate region if the RRJPNN control cannot be guaranteed.

To fulfill the remunerated mechanism, a minimum difference  $\lambda$  can be described as

$$\lambda = (l_x - l_x^*) - (l_x - l_v^*) \tag{22}$$

where  $l_x^* = d_t^* = (\mathbf{C}^*)^T \mathbf{D}$  is the excellent control rule of the RRJPNN control;  $\mathbf{C}^*$  is the excellent weight vector;  $|\lambda| < \gamma < \delta$ ,  $\delta + ((R_v(\mu_v) + R_b + |d\mu_v/dt| + |c_v s_a|)/h_x) > 0$  and  $\delta$  are greater than zero. By using Equation (22),  $l_x = d_t^3(K) = \mathbf{C}^T \mathbf{D}$  and  $l_x^* = (\mathbf{C}^*)^T \mathbf{D}$ , then Equation (16) can be described as

$$\begin{aligned} \frac{ds_a}{dt} &= h_x l_v^* - h_x l_x - h_x l_y - h_x l_z - h_x l_w - c_v s_a \\ &= h_x [(l_x - l_x^*) - (l_x - l_v^*)] + h_x (l_x^* - l_x) - h_x l_y - h_x l_z - h_x l_w - c_v s_a \\ &= h_x \lambda + h_x [(\mathbf{C}^*)^T \mathbf{D} - \mathbf{C}^T \mathbf{D}] - h_x l_y - h_x l_z - h_x l_w - c_v s_a \end{aligned} \tag{23}$$

To obtain two remunerated controls, the attunement law and the two evaluation laws, the Lyapunov function is described as

$$V_x = \frac{s_a^2}{2} + \frac{(\mathbf{C}^* - \mathbf{C})^T (\mathbf{C}^* - \mathbf{C})}{2v_1} + \frac{(\hat{\gamma} - \gamma)^2}{2\tau_1} + \frac{(\hat{\delta} - \delta)^2}{2\tau_2} \tag{24}$$

where  $v_1$  is the learning rate of the conjoined weight;  $\tau_1$  and  $\tau_2$  are the two positive evaluation rates;  $\hat{\gamma} - \gamma$  and  $\hat{\delta} - \delta$  are the evaluation differences. By using Equations (22) and (23), then the differential equation of (24) can be described as

$$\begin{aligned} \frac{dV_x}{dt} &= s_a \frac{ds_a}{dt} - \frac{(\mathbf{C}^* - \mathbf{C})^T}{v_1} \frac{d\mathbf{C}}{dt} + (\hat{\gamma} - \gamma) \frac{d(\hat{\gamma} - \gamma)}{\tau_1 dt} + (\hat{\delta} - \delta) \frac{d(\hat{\delta} - \delta)}{\tau_2 dt} \\ &= s_a \{ h_x \lambda + h_x [(\mathbf{C}^* - \mathbf{C})^T \mathbf{D}] - h_x l_z - h_x l_w - h_x l_x - c_v s_a \} - \frac{(\mathbf{C}^* - \mathbf{C})^T}{v_1} \frac{d\mathbf{C}}{dt} + (\hat{\gamma} - \gamma) \frac{d\hat{\gamma}}{\tau_1 dt} + (\hat{\delta} - \delta) \frac{d\hat{\delta}}{\tau_2 dt} \end{aligned} \tag{25}$$

The attunement law  $\frac{d\mathbf{C}}{dt}$ , two remunerated controls,  $l_z$  and  $l_w$ , and two evaluation laws,  $d\hat{\gamma}/dt$  and  $d\hat{\delta}/dt$  to fulfill  $\frac{dV_x}{dt} \leq 0$  can be described as

$$\frac{d\mathbf{C}}{dt} = v_1 s_a h_x \mathbf{D} \tag{26}$$

$$l_z = \hat{\gamma} \text{sgn}(s_a h_x) \tag{27}$$

$$l_w = \hat{\delta} \text{sgn}(s_a h_x) \tag{28}$$

$$\frac{d\hat{\gamma}}{dt} = \tau_1 |s_a h_x| \tag{29}$$

$$\frac{d\hat{\delta}}{dt} = \tau_2 |s_a h_x| \tag{30}$$

By using Equations (26)–(30) and (17), then Equation (25) can be rewritten by

$$\begin{aligned} \frac{dV_x}{dt} &= s_a \{h_x \lambda + h_x [(\mathbf{C}^* - \mathbf{C})^T \mathbf{D}] - h_x l_y - h_x l_z - h_x l_w - c_v s_a\} - \frac{(\mathbf{C}^* - \mathbf{C})^T d\mathbf{C}}{v_1} + (\hat{\gamma} - \gamma) \frac{d\hat{\gamma}}{\tau_1 dt} + (\hat{\delta} - \delta) \frac{d\hat{\delta}}{\tau_2 dt} \\ &= -c_a s_a^2 + s_a h_x \{ \lambda + (\mathbf{C}^* - \mathbf{C})^T \mathbf{D} - (\hat{\gamma} + \hat{\delta}) \text{sgn}(s_a h_x) - \frac{1}{h_x} [ \left| \frac{d\mu_v}{dt} \right| + |c_v s_a| + R_a(\mu_v) + R_b ] \text{sgn}(s_a h_x) \} \\ &\quad - \frac{(\mathbf{C}^* - \mathbf{C})^T}{v_1} v_1 s_a h_x \mathbf{D} + (\hat{\gamma} - \gamma) \frac{\tau_1 |s_a h_x|}{\tau_1} + (\hat{\delta} - \delta) \frac{\tau_2 |s_a h_x|}{\tau_2} \\ &= -c_a s_a^2 + (s_a h_x \lambda - \gamma |s_a h_x|) - \{ \delta + \frac{1}{h_x} [ \left| \frac{d\mu_v}{dt} \right| + |c_v s_a| + R_v(\mu_v) + R_b ] \} |s_a h_x| \end{aligned} \tag{31}$$

By using  $|\lambda| < \gamma < \delta$  and  $\delta + ((R_v(\mu_v) + R_b + |d\mu_v/dt| + |c_v s_a|)/h_x) > 0$ , then Equation (31) can be rewritten by

$$\begin{aligned} \frac{dV_x}{dt} &\leq -c_v s_a^2 + (|\lambda| - \gamma) |s_a h_x| \\ &\leq -c_v s_a^2 \\ &\leq 0 \end{aligned} \tag{32}$$

$s_a$  and  $(\mathbf{C}^* - \mathbf{C})$  are represented as bounded when  $\frac{dV_x}{dt} \leq 0$ , which is a negative semidefinite. Additionally, the uniformly continuous function  $x_a(t)$  can be described by

$$x_a(t) = -\frac{dV_x}{dt} = c_v s_a^2 \tag{33}$$

The integral of  $x_a(t)$  can be rewritten by

$$\int_0^t x_a(\varepsilon) d\varepsilon = \int_0^t \left[ -\frac{dV_x}{d\varepsilon} \right] d\varepsilon = V_x(0) - V_x(t) \tag{34}$$

The differential of Equation (33) can be described as

$$\frac{dx_a(t)}{dt} = 2c_v s_a \frac{ds_a}{dt} \tag{35}$$

The limitation of Equation (34) when  $V_x(0)$  and  $V_x(t)$  are bounded can be described as

$$\lim_{t \rightarrow \infty} \int_0^t x_a(\varepsilon) d\varepsilon < \infty \tag{36}$$

As all variables on the right side of Equation (23) are bounded, which implies  $\frac{ds_a}{dt}$  is also bounded and it can be shown that  $\lim_{t \rightarrow \infty} \int_0^t x_a(\varepsilon) d\varepsilon = 0$ , thus  $s_a(t) \rightarrow 0$  as  $t \rightarrow \infty$  by using Barbalat’s lemma [36,37]. Therefore, the proposed witty control system is gradually stable from proof. Moreover, the tracking error  $s_a(t)$  of the system will converge to zero.

Therefore, to describe the online training process of the RRJPNN, an objective function can be defined by

$$V_y = \frac{s_a^2}{2} \tag{37}$$

The conjoined weight by using the backpropagation technology and the gradient descent technology from the attunement law  $\frac{d\mathbf{C}}{dt}$  can be described as

$$\frac{d\rho_{ts}^2}{dt} = v_1 s_a h_x q_t^3 \tag{38}$$

By using the two above technologies, the conjoined weight from Equation (38) can be expressed by

$$\frac{d\rho_{ts}^2}{dt} = -v_1 \frac{\partial F_2}{\partial \rho_{ts}^2} = -v_1 \frac{\partial V_y}{\partial s_a} \frac{\partial s_a}{\partial d_t^3} \frac{\partial d_t^3}{\partial b_t^3} \frac{\partial b_t^3}{\partial \rho_{ts}^2} = -v_1 \frac{\partial V_y}{\partial d_t^3} \frac{\partial d_t^3}{\partial b_t^3} \frac{\partial b_t^3}{\partial \rho_{ts}^2} = -v_1 q_t^3 \frac{\partial V_y}{\partial d_t^3} \quad (39)$$

In comparison with Equations (38) and (39), this can be obtained as

$$\frac{\partial V_y}{\partial d_t^3} = -s_a h_x \quad (40)$$

The updated law of the conjoined weight can be denoted by [38]

$$\rho_{ts}^2(K+1) = \rho_{ts}^2(K) + \frac{d\rho_{ts}^2}{dt} \quad (41)$$

By using the two above technologies, the recurrent weight of the attunement law can be expressed by

$$\frac{d\rho_{rt}^1}{dt} = -v_2 \frac{\partial V_y}{\partial d_t^3} \frac{\partial d_t^3}{\partial d_s^2} \frac{\partial d_s^2}{\partial b_s^2} \frac{\partial b_s^2}{\partial d_r^1} \frac{\partial d_r^1}{\partial b_r^1} \frac{\partial b_r^1}{\partial \rho_{rt}^1} = v_2 h_x s_a \rho_{ts}^2 P_s(\cdot) q_r^1(K) d_t^3(K-1) d_r^1(K) \quad (42)$$

where  $v_2$  is the learning rate of the recurrent weight. The updated law of the recurrent weight can be denoted by [38]

$$\rho_{rt}^1(K+1) = \rho_{rt}^1(K) + \frac{d\rho_{rt}^1}{dt} \quad (43)$$

Moreover, the ABSA method was applied to search for two optimal adjustable learning rates and to improve convergent speed of the weights in the RRJPNN in this research. The existing algorithm with the excellent behavior of miniature bat echolocation is the important development of the BA method. By adopting a random technology, this algorithm produces a set of solutions. Then, the optimal solution is found by using the loop search. The local solution is generated by random flight and generates a global optimal solution. For all bats, the position of the bat  $i$  is  $z_i(n-1)$ , the flight velocity is  $f_i(n-1)$  and the current global optimal position is  $z^*$  when their foraging space is part of the  $d$ -dimension at  $n-1$  time. The flight velocity  $f_i(n)$  and position  $z_i(n)$  of bat  $i$  at  $n$  time can be calculated by

$$k_i = k_{\min} + (k_{\max} - k_{\min})n/N_{\max}, \quad i = 1, 2 \quad (44)$$

$$f_i(n) = f_i(n-1) + (z_i(n-1) - z^*)k_i, \quad i = 1, 2, n = 1, \dots, j \quad (45)$$

$$z_i(n) = z_i(n-1) + f_i(n), \quad i = 1, 2, n = 1, \dots, j \quad (46)$$

where  $N_{\max}$  is the maximum number of iterations;  $k_{\max}$  and  $k_{\min}$  are the maximum and minimum frequencies of the soundwaves produced by the bat. In the initial process, the frequency of the bat's soundwaves is uniformly distributed between  $k_{\min} = 0$  and  $k_{\max} = 1$ . The concerning frequency is obtained by adopting Equation (44). By adopting Equations (45) and (46), the local search is realized. The bat randomly goes along the optimal solution, and the new solution is updated by

$$z_{new}(n) = z_{old}(n-1) + \sigma \times \bar{d}_i(n), \quad i = 1, 2, n = 1, \dots, j \quad (47)$$

where  $\sigma$  is a random number at  $[-1, 1]$ .  $z_{old}(n-1)$  is the solution selected from the current optimal solution by adopting a random skill.  $\bar{d}_i(n)$  is the average loudness from the bat generation at  $n$  time. Additionally, it achieves a global search by controlling modified

loudness  $d_i(n+1)$  and modified pulse rate  $e_i(n+1)$ . The modified pulse rate  $e_i(n+1)$  and modified loudness  $d_i(n+1)$  of the bat launch pulse can be updated by

$$e_i(n+1) = [e_i(n) - e_i(0)][1 - \exp(-n\zeta)], \quad i = 1, 2, n = 1, \dots, j \quad (48)$$

$$e_i(n)^{d_i(n+1)} = \zeta[d_i(n) - d_i(0)], \quad i = 1, 2, n = 1, \dots, j \quad (49)$$

where  $e_i(0)$  is an initial rate and  $d_i(0)$  is an initial loudness.  $\zeta$  is a constant between 0 and 1 and  $\zeta$  is a positive constant. When the bat is conscious of the presence of the prey, it will increase its pulse emission rate and reduce the response of its pulsed emission. At last,  $z_i(n)$ ,  $i = 1, 2$  is the best solution concerning the learning rates  $v_i(n)$ ,  $i = 1, 2$  of the two weights in the RRJPNN. Thereby, the two adjustable values may be optimized by adopting ABSA method to find the two learning rates of weights. Moreover, a progressive weight pruning approach is based on the ABSA method to quicken convergence of weight.

#### 4. Tests and Results

The arrangement of the ISM driving the rice milling machine system by adopting a DSP control system is illustrated in Figure 1. In Figure 5, an experimental photo of the ISM and the rice milling machine system is illustrated.

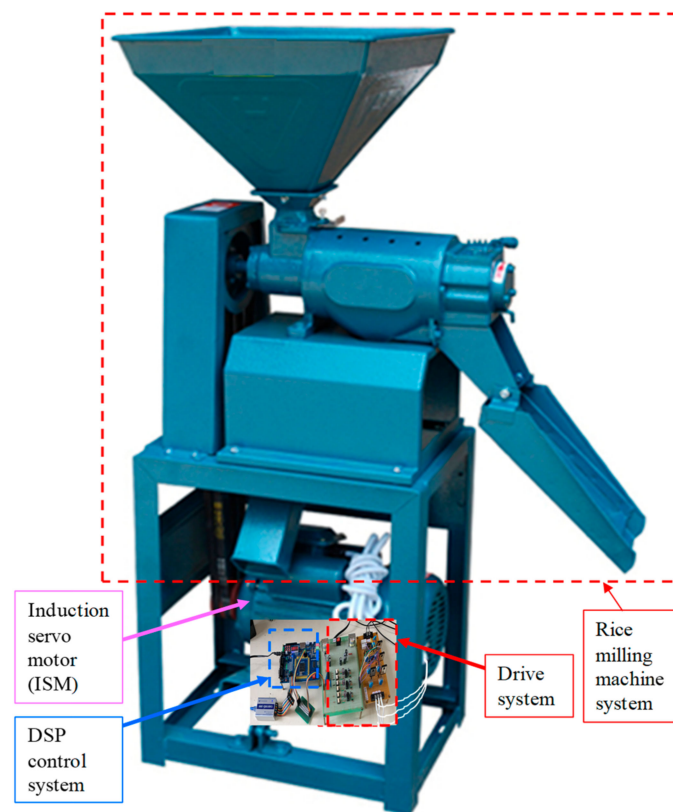


**Figure 5.** An experimental photo of the ISM and the rice milling machine system.

The conversion ratio for the rice milling machine system is 2.2. The profile formats are the belt 1 length is 42.2 mm, the belt 2 length is 52.2 mm, the main idler diameter is 92.6 mm, the diameter of idler 1 is 45.2 mm, and the diameter of idler 2 is 64.2 mm. The specification of the ISM is three-phase two-pole 220 V, 60 Hz, 3 kW, 3582 rpm. The position and speed conversion ratios are 1 V = 50 rad and 1 V = 50 rad/s. The internal parameters of the ISM are  $r_a = 1.08 \Omega$ ,  $r_b = 1.02 \Omega$ ,  $L_u = 8.65 \text{ mH}$ ,  $L_v = 10.68 \text{ mH}$ ,  $L_{uv} = 8.89 \text{ mH}$ ,  $f_a = 16.22 \times 10^{-3} \text{ Nms}^2 = 0.811 \text{ Nmsrad/V}$ , and  $g_a = 1.12 \times 10^{-3} \text{ Nms/rad} = 0.056 \text{ Nm/V}$ . Figure 6 illustrates the control flowchart of executive program by adopting the DSP control system.

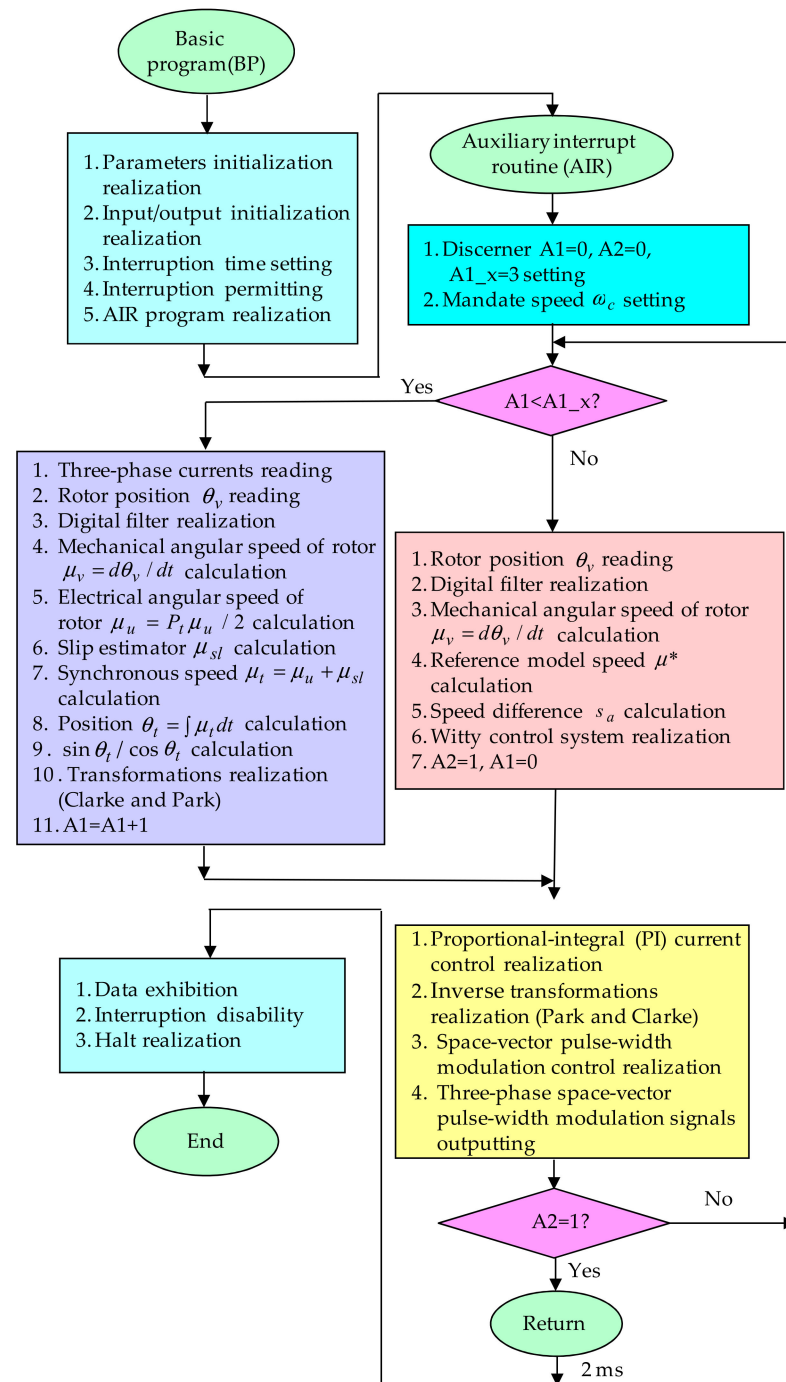


**Figure 6.** Control flowchart of executive program.

The program in the experimental tests consists of the basic program (BP) and the auxiliary interrupt routine (AIR). The BP conducts all initializations for the adopted parameters and all settings for the input/output interfaces. The AIR achieves the interrupt execution within 2 ms. The executed processes by AIR are as follows: three-phase currents read from analog–digital conversions, rotor position read from encoder interface circuit, rotor speed computation, speed difference computation, lookup table generation, coordinate transformations realization, PI current control realization, the proposed control system realization, and three-phase space-vector pulse-width-modulation outputs for switching the voltage fed converter. Three discerners  $A1_x$ ,  $A1$ ,  $A$  and  $2$  are set as 3, 0 and 0, respectively. The DSP control system with the IFOC applied the discerner  $A2$  to act as the executing number of the proposed control method. If the IFOC is executed less than three times, i.e.,

$A1 < A1_x$ , the IFOC needs to be enforced repeatedly. The proposed control method is executed one time and the IFOC is executed three times. Then, the AIR will back to the BP.

The experimental results with three test examples are shown to show some of the control performances. Firstly, test JA is the case with huge comprehensive coalescence disturbances and parameter variations  $\Delta F_a + F_{b1}$  at 1.2 s, starting with a mandate speed of 1600 rpm (167.47 rad/s). Secondly, test JB is the case with double huge comprehensive coalescence disturbances and parameter variations  $\Delta F_a + F_{b1}$  at 1.2 s, starting with a mandate speed of 3300 rpm (345.40 rad/s). Thirdly, test JC has a mandate speed of 2000 rpm (209.33 rad/s) starting at 2 s and a mandate speed of 3000 rpm (314.00 rad/s) at 10 s, with acceleration and added external load torque disturbance and parameter variations  $8 Nm(F_{1c}) + F_{b1}$  at 14 s, with a mandate speed of 3000 rpm (314.00 rad/s). The PI controller as the TA controller and the proposed witty control system as the TB controller are the two adopted controllers that are compared with control performances. Firstly, two gains of the PI control as the TA controller are the proportional gain of 24.1 and the integral gain of 10.2 by adopting the heuristic method [30–32] to obtain finer dynamic response under the requirement of stability consideration. The control gains by using the proposed witty control system as the TB controller are given as  $c_v = 5.41$ ,  $\chi = 0.092$ ,  $\tau_1 = 0.12$  and  $\tau_2 = 0.13$  to better measure transient performance under the demand of stability planning. In addition, the number of nodes of the RRJPNN, by adopting the progressive weight pruning approach based on ABSA method to quicken convergence of conjoined weight, are 2, 4 and 1 in the forehead, center and readward layers to better measure transient-state and steady-state control properties.

Firstly, Figure 7a,b display speed responses for measured speed  $\mu_v$ , mandate speed  $\mu_c$  and reference model speed  $\mu^*$  via experimental results of test JA by adopting the TA and TB controllers for the ISM driving the rice milling machine system.

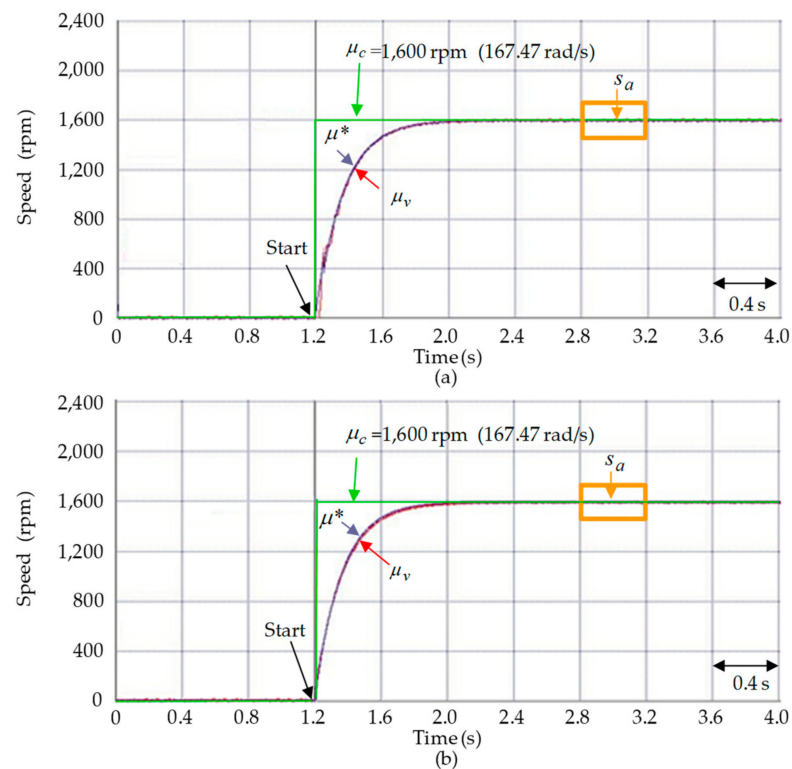


**Figure 7.** Speed responses via experimental results for the ISM driving the rice milling machine system at test JA by adopting the controllers: (a) TA; (b) TB.

Figure 8a,b display increase in speed difference  $s_a$  responses between 2.8 and 3.2 s via experimental results at test JA by adopting the TA and TB controllers for the ISM driving the rice milling machine system.

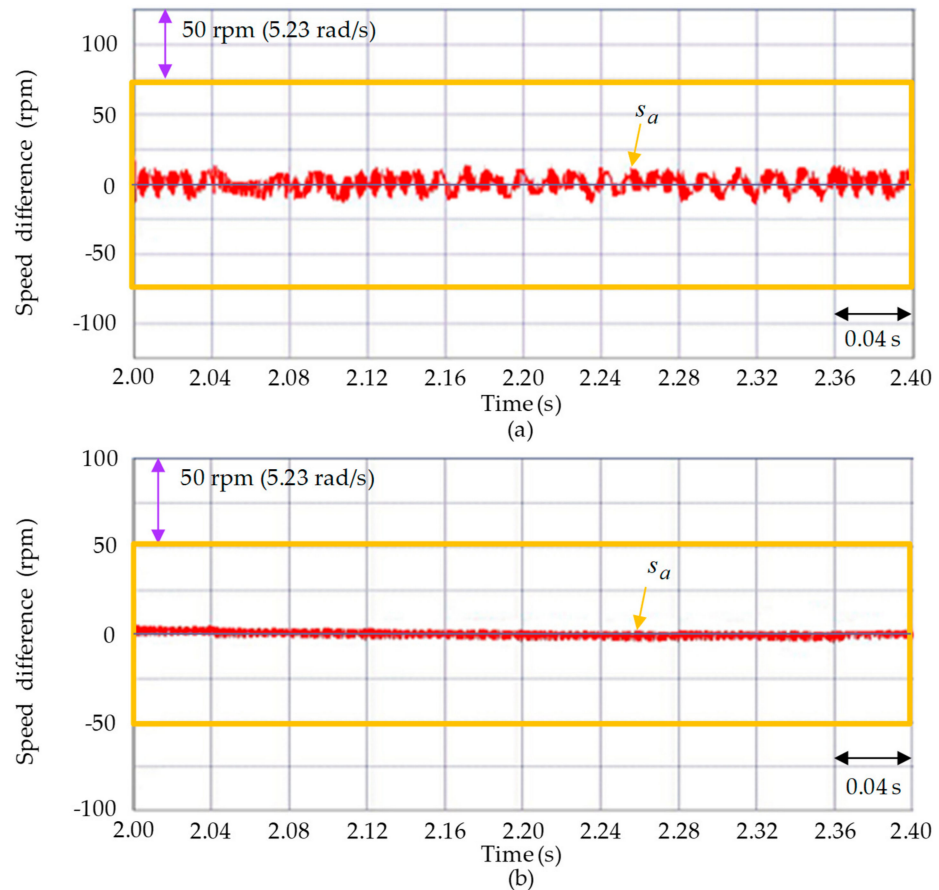
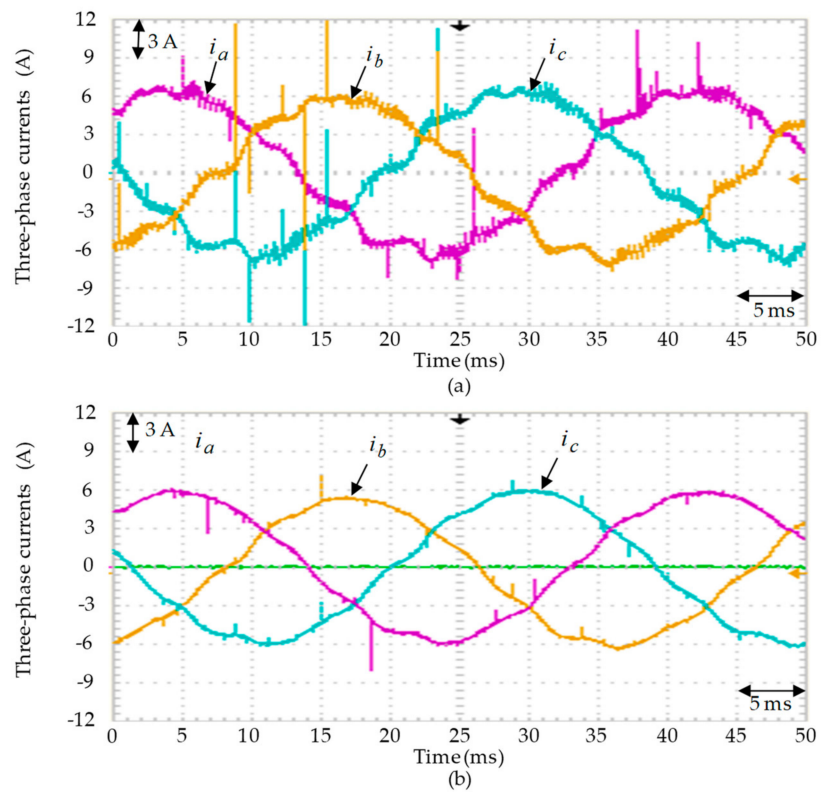


**Figure 8.** Increase in speed difference responses via experimental results for the ISM driving the rice milling machine system at test JA by adopting the controllers: (a) TA; (b) TB.

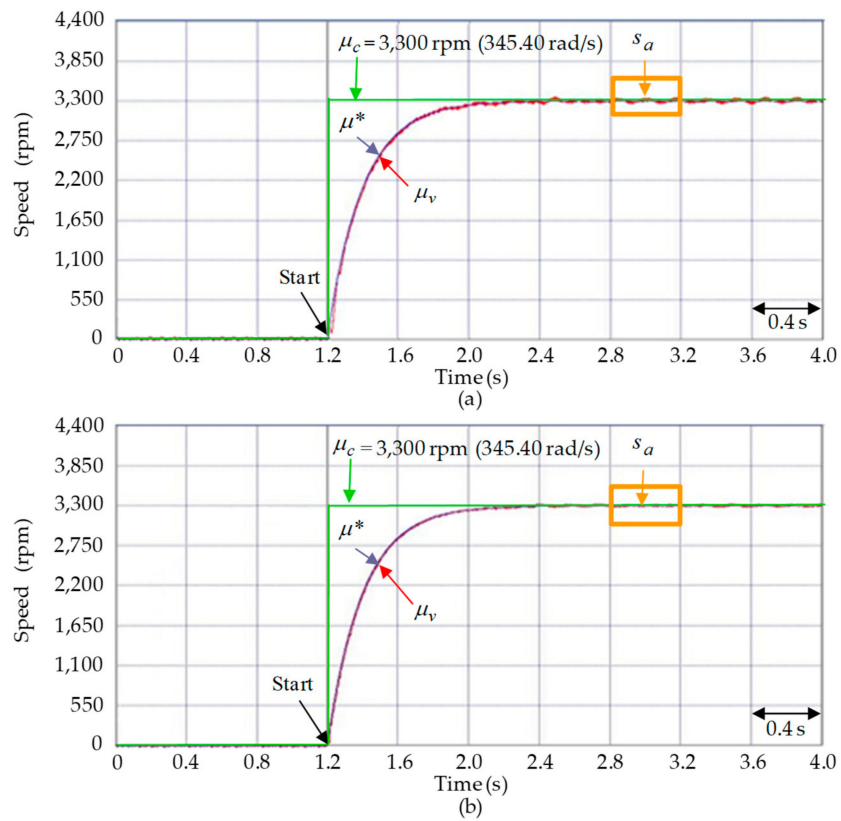
Figure 9a,b display the responses of three-phase currents via experimental results at test JA by adopting the TA and TB controllers for the ISM driving the rice milling machine system.

Figure 7a,b show that by adopting the TA and TB controllers in test JA, a better speed tracking performance was achieved because of smaller disturbance. However, the increase in tracking error when adopting the TA controller shown in Figure 8a is larger than the increase in tracking error when adopting the TB controller shown in Figure 8b. The response of three-phase currents when adopting the TA controller shown in Figure 9a generates a larger harmonic wave than when adopting the TB controller shown in Figure 9b.

Secondly, Figure 10a,b display speed responses for measured speed  $\mu_v$ , mandate speed  $\mu_c$  and reference model speed  $\mu^*$  via experimental results of test JB by adopting the TA and TB controllers for the ISM driving the rice milling machine system.



**Figure 9.** Responses of three-phase currents via experimental results for the ISM driving the rice milling machine system in test JA by adopting the controllers: (a) TA; (b) TB.



**Figure 10.** Speed responses via experimental results for the ISM driving the rice milling machine system in test JB by adopting the controllers: (a) TA; (b) TB.

Figure 11a,b display in increase speed difference  $s_a$  responses between 2.8 s and 3.2 s via experimental results at test JB by adopting the TA and TB controllers for the ISM driving the rice milling machine system.

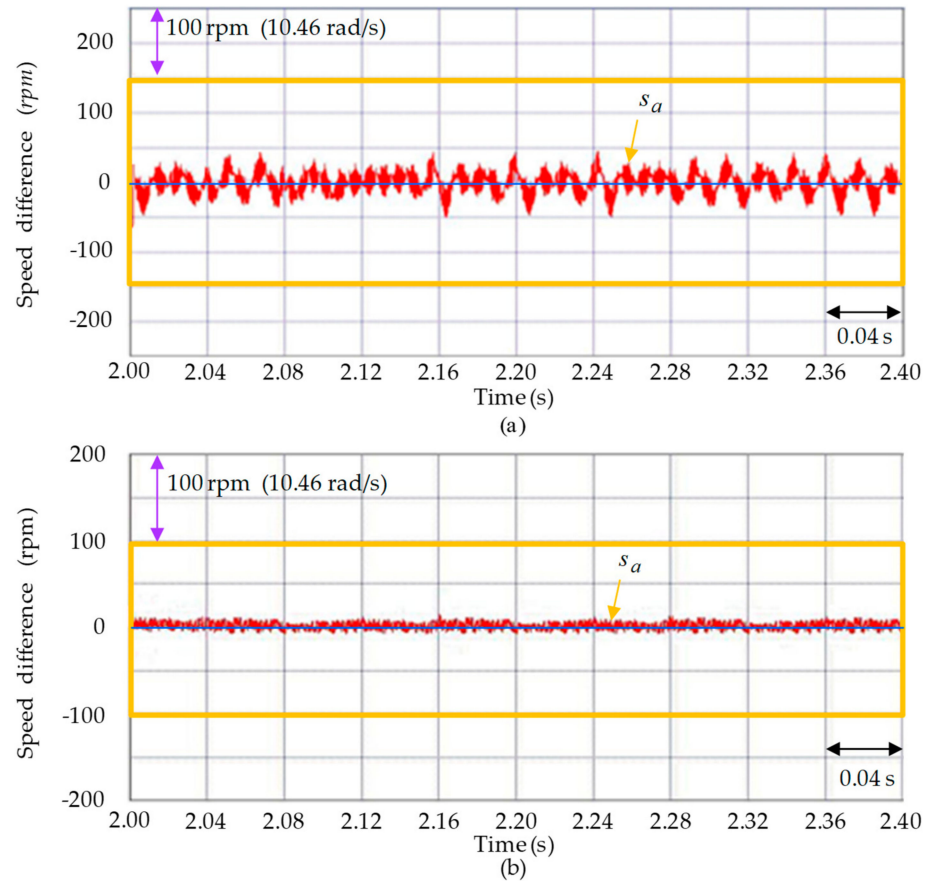
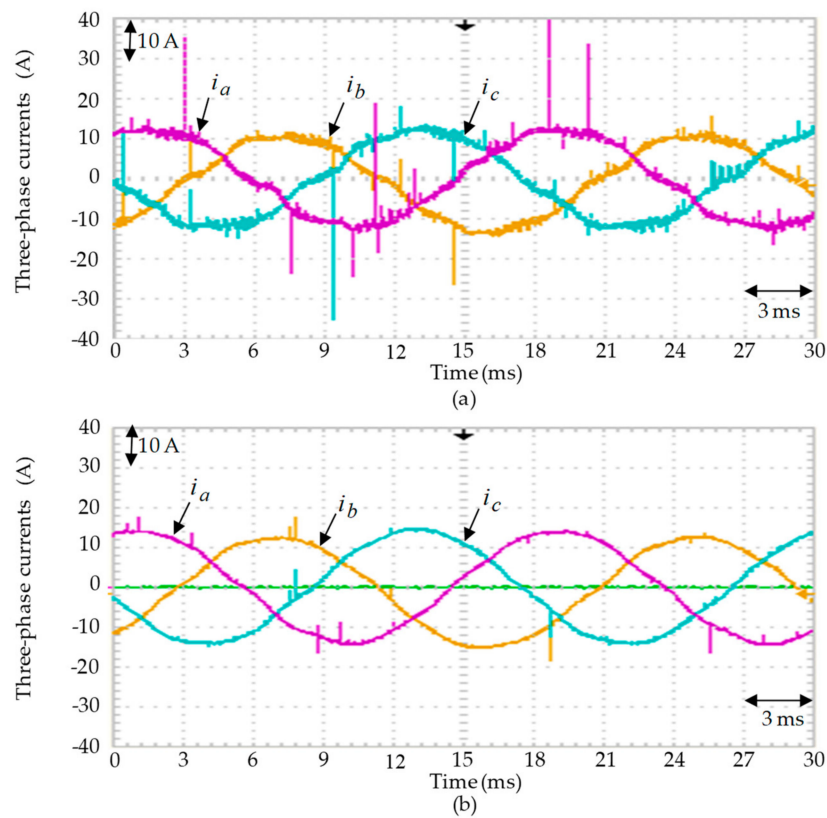


**Figure 11.** Increase in speed difference responses via experimental results for the ISM driving the rice milling machine system in test JB by adopting the controllers: (a) TA; (b) TB.

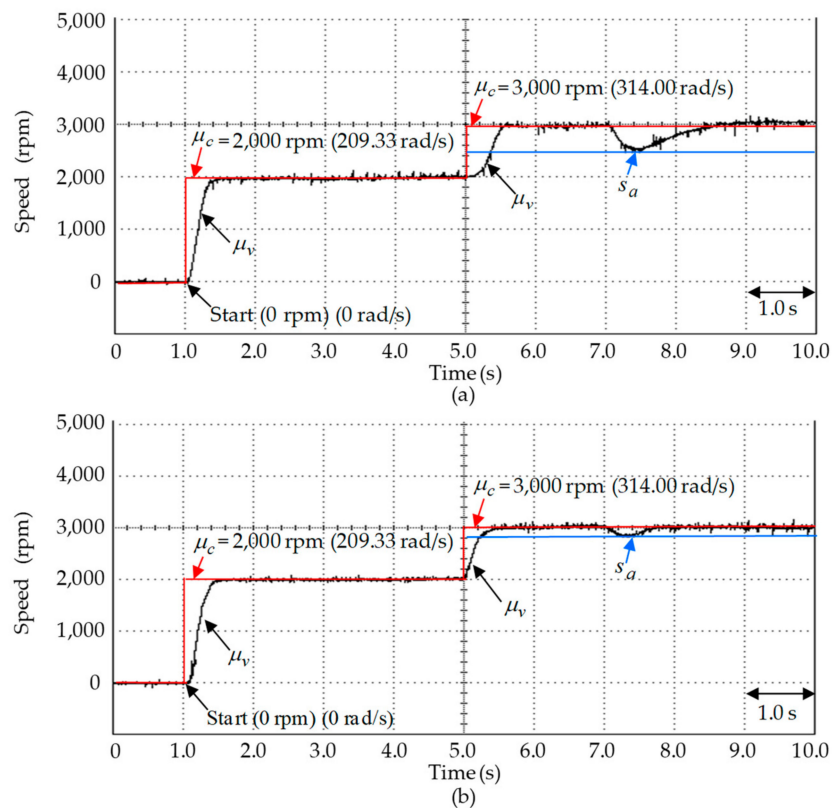
Figure 12a,b display responses of three-phase currents via experimental results of test JB by using the controllers TA, and TB for the ISM driving the rice milling machine system.

Figure 10a by using the TA controller in test JB appeared to show a dilatory speed response because of no good gain adjustment in the TA controller. In Figure 10b, by adopting the TB controller at test JB, a good speed response is demonstrated, owing to online adjustable method of RRJPNN control and two remunerated controls. However, the increase in tracking error when adopting the TA controller shown in Figure 11a is larger than the increase in tracking error when adopting the TB controller shown in Figure 11b. The response of three-phase currents when adopting the TA controller shown in Figure 12a results in larger harmonics than when adopting the TB controller shown in Figure 12b.

Thirdly, Figure 13a,b display two various speed-regulated responses when adding load torque via experimental results of test JC by using the TA and TB controllers for the ISM driving the rice milling machine system.



**Figure 12.** Responses of three-phase currents via experimental results for the ISM driving the rice milling machine system at test JA by adopting the controllers: (a) TA; (b) TB.



**Figure 13.** Two speed-regulated responses when adding load torque via experimental results of test JC by adopting the controllers: (a) TA; (b) TB.

Figure 14a,b display responses of three-phase currents with addition of load torque via experimental results of test JC by using the TA and TB controllers for the ISM driving the rice milling machine system.

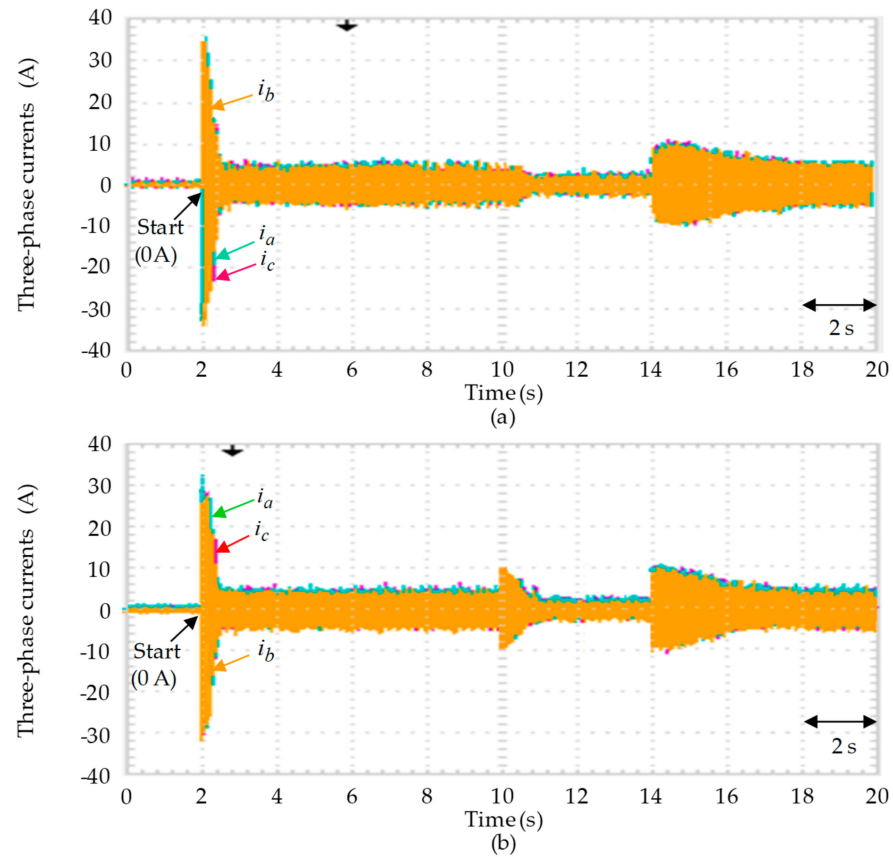


**Figure 14.** Responses of three-phase currents with adding load torque via experimental results of test JC by adopting the controllers: (a) TA; (b) TB.

The two speed-regulated responses when adding load torque via experimental results by adopting the TA controller, shown in Figure 13a, are worse than the two speed-regulated responses when adding load torque via experimental results by using the TB controller, also shown in Figure 13a. Responses of three-phase currents with adding load torque via experimental results by adopting the TA controller shown in Figure 14a has a greater harmonic than responses of three-phase currents when adding load torque via experimental results by adopting the TB controller shown in Figure 14b.

Moreover, responses of the two learning rates curves in test JB shown in Figure 15a,b using calculated learning rates according to the proposed ABSA method are compared to two learning rates of conjoined weight and recurrent weight by utilizing the PSO method [20] and ACO method [23] to demonstrate the usefulness of this novel technique. This study shows that convergence to optimal values can be achieved by using the proposed ABSA method. The proposed method also achieves faster convergence and less computational complexity.

Additionally, responses of two weights at test JB by using the PSO method [20] and the ACO method [23] and the proposed ABSA method are shown in Figure 16a,b. The convergences of conjoined weight and recurrent weight by using the proposed ABSA method with progressive weight pruning approach are superior to the ACO method and the PSO method. Thereby, the proposed method with progressive weight pruning approach can quicken convergence of weights.

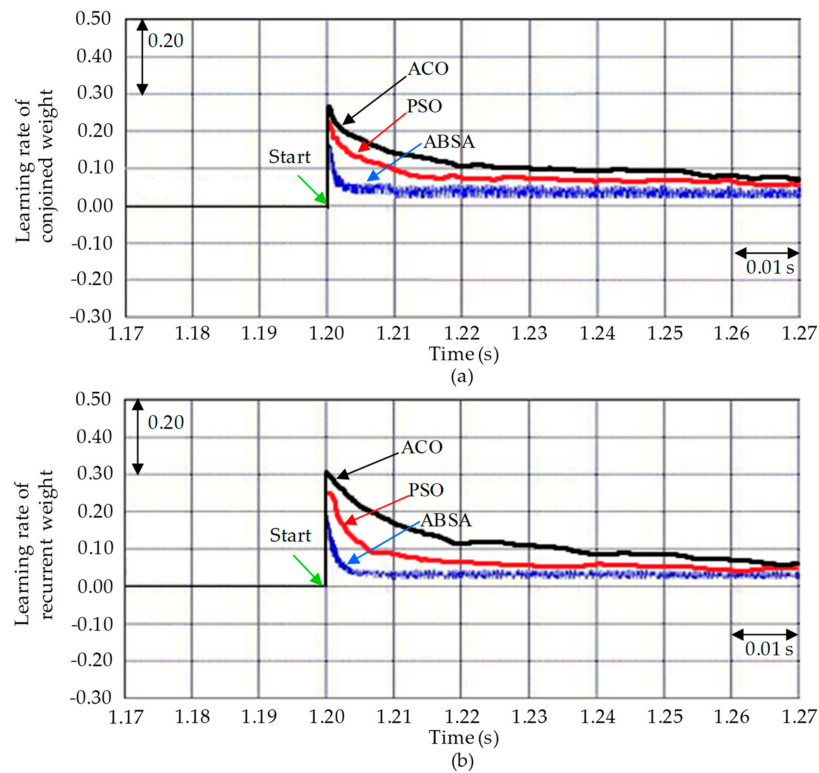


**Figure 15.** Responses of two learning rates via experimental results of test JB by adopting the ant colony algorithm (ACO), particle swarm optimization (PSO) and altered bat search algorithm (ABSA) methods for: (a) learning rate of conjoined weight, (b) learning rate of recurrent weight.

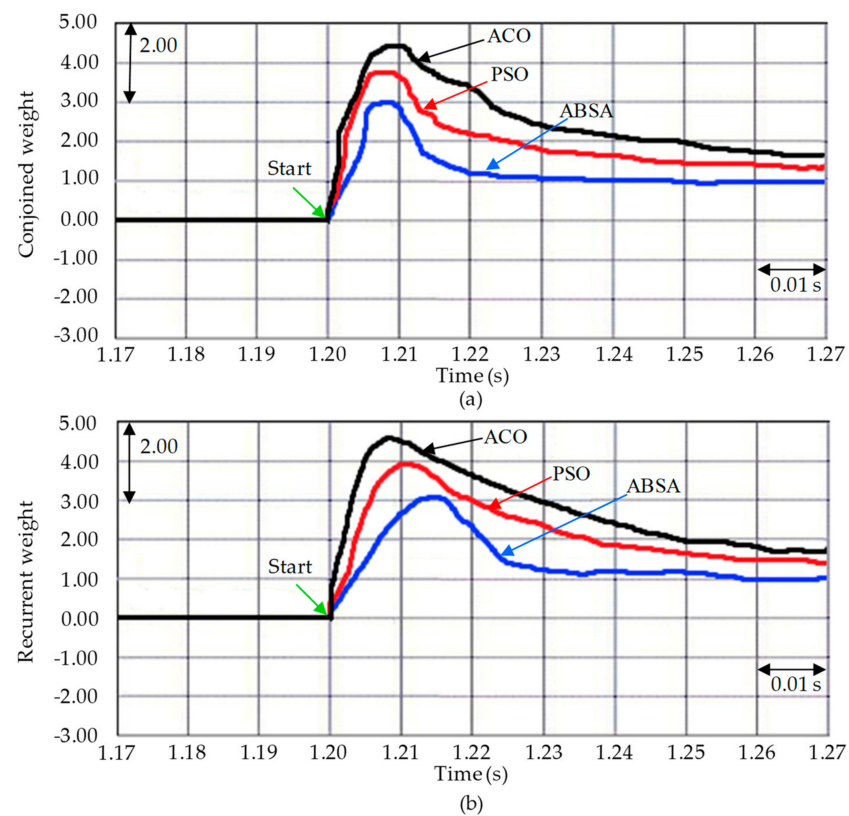


**Figure 16.** Responses of two weights via experimental results of test JB by adopting the ACO, PSO and ABSA methods for: (a) conjoined weight; (b) recurrent weight.

Furthermore, response of the numbers of conjoined weight at test JB by using the PSO method [20] and the ACO method [23] and the proposed ABSA method by adopting the progressive weight pruning approach is shown in Figure 17. The convergence of numbers of conjoined weight by using the proposed ABSA method and the progressive weight pruning approach is superior to the ACO method and the PSO method. Thereby, the proposed method can achieve faster convergence in conjoined weight.

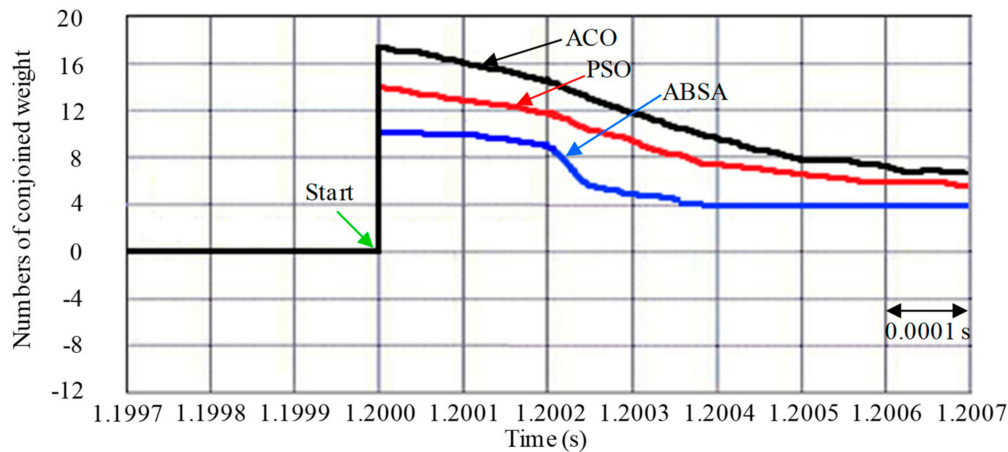


**Figure 17.** Responses of numbers of conjoined weight via experimental results of test JB by adopting the ACO, PSO and ABSA methods.

### 5. Analyses and Discussion

Dynamic responses for the PI controller as the TA controller and the proposed witty control system as the TB controller at three tested examples via experimental results that are listed in Table 1 are explained as below. For test JA, the maximum differences for the TA and TB controllers are 82 (8.58 rad/s) and 30 rpm (3.14 rad/s), and the quadratic mean differences for the TA and TB controllers are 48 (5.02 rad/s) and 17 rpm (1.78 rad/s). For test JB, the maximum differences for the TA and TB controllers are 128 (13.40 rad/s) and 35 rpm (3.66 rad/s), and the quadratic mean differences for the TA and TB controllers are 53 (5.55 rad/s) and 19 rpm (1.99 rad/s). For test JC, the maximum differences for the TA and TB controllers are 489 (51.18 rad/s) and 192 rpm (20.10 rad/s), and the quadratic mean differences for the TA and TB controllers are 188 (19.68 rad/s) and 46 rpm (4.81 rad/s). The TB controller has better dynamic responses than the TA controller according to the experimental results in tests JA, JB and JC.

**Table 1.** Dynamic responses for the two controllers.

Three Test Examples	Controllers Performance	TA Controller		TB Controller	
		Maximum Differences of $s_a$	Quadratic Mean Differences of $s_a$	Maximum Differences of $s_a$	Quadratic Mean Differences of $s_a$
Test JA		82 rpm (8.58 rad/s)	48 rpm (5.02 rad/s)	30 rpm (3.14 rad/s)	17 rpm (1.78 rad/s)
Test JB		128 rpm (13.40 rad/s)	53 rpm (5.55 rad/s)	35 rpm (3.66 rad/s)	19 rpm (1.99 rad/s)
Test JC		489 rpm (51.18 rad/s)	188 rpm (19.68 rad/s)	192 rpm (20.10 rad/s)	46 rpm (4.81 rad/s)

Additionally, the peculiarity performances for the TA and TB controllers according to the three tested examples via experimental results that are listed in Table 2 are represented as below. The total harmonic distortion (THD) values in the three-phase currents for the TA and TB controllers in test JB are 21% and 5%. The responses of rising times for the TA and TB controllers in test JB are 0.92 s and 0.75 s. The regulation capabilities with

adding load torque for the TA and TB controllers in test JC are 489 rpm (51.18 rad/s) in maximum difference and 192 rpm (20.10 rad/s) in maximum difference. The speed tracking differences for the TA and TB controllers in test JB are 128 rpm (13.40 rad/s) in maximum difference and 35 rpm (3.66 rad/s) in maximum difference. The denial potentialities of parameter disturbance for the TA and TB controllers in test JB are 128 rpm (13.40 rad/s) in maximum difference and 35 rpm (3.66 rad/s) in maximum difference. The above performances concerning the harmonic values in the three-phase currents, the dynamic responses, the regulation capabilities for adding load torque, the speed tracking differences and the denial potentialities of parameter disturbance in the TB controller are better than the TA controller. Thereby, the TB controller has better peculiarity performance than the TA controller from experimental results of tests JB and JC.

**Table 2.** Peculiarity performances for the two controllers.

Peculiarity Performances	Controllers	TA Controller	TB Controller
Total harmonic distortion (THD) values in the three-phase currents in test JB		21%	5%
Responses of rising times in test JB		0.92 s	0.75 s
Regulation capabilities with adding load torque in test JC		489 rpm (51.18 rad/s) in maximum difference	192 rpm (20.10 rad/s) in maximum difference
Speed tracking differences in test JB		128 rpm (13.40 rad/s) in maximum difference	35 rpm (3.66 rad/s) in maximum difference
Denial potentialities of parameter disturbance in test JB		128 rpm (13.40 rad/s) in maximum difference	35 rpm (3.66 rad/s) in maximum difference

## 6. Conclusions

The proposed witty control system has been applied to control the the ISM driving the rice milling machine system with better robustness. The proposed witty control system that can realize the RRJPNN control, which involves an attunement law, two remunerated controls, which have two evaluation laws, and a dominator control were proposed to obtain a fine control performance.

The contributions of this research are as below. (a) The dynamic models of the ISM driving the rice milling machine system have been developed. (b) The ISM driving the rice milling machine system under huge comprehensive nonlinear synthesized disturbances and parameter variations affect has been controlled by using the proposed witty control method. (c) On the basis of the Lyapunov stability principle, the attunement law in the RRJPNN control and the two evaluation laws in the two remunerated controls have been developed. (d) The ABSA method was utilized to find the learning rates of conjoined and recurrent weights in the RRJPNN to obtain optimal values and to quicken convergence of weights. (e) The proposed witty control system has better sinusoidal shapes than the PI control in terms of the harmonics values of three-phase currents.

Finally, all results show that the proposed witty control system is better than the PI control for the ISM driving the rice milling machine system from all experimental results and control behaviors.

**Author Contributions:** Conceptualization, D.-F.C., S.-P.-C.C., A.-B.C. and J.-C.T.; methodology, S.-P.-C.C.; software, S.-P.-C.C. and A.-B.C.; validation, S.-P.-C.C. and J.-C.T.; formal analysis, S.-P.-C.C. and A.-B.C.; investigation, S.-P.-C.C. and J.-C.T.; writing—original draft preparation, S.-P.-C.C. and J.-C.T.; writing—review and editing, S.-P.-C.C. and J.-C.T. All authors have read and agreed to the published version of the manuscript.

**Funding:** This research received no external funding.

**Institutional Review Board Statement:** Not applicable.

**Informed Consent Statement:** Not applicable.

**Data Availability Statement:** Data is contained within the article.

**Conflicts of Interest:** The authors declare no conflict of interest.

## Abbreviations

$w_u, w_v$	$u - v$ axis stator voltages
$q_u, q_v$	$u - v$ axis stator currents
$q_{ur}, q_{vr}$	$u - v$ axis rotor currents
$L_u, L_v, L_{uv}$	$u - v$ axis self inductances, mutual inductance
$r_a, r_b$	stator and equalized rotor resistances.
$\mu_v, \mu_u, \mu_t$	mechanical and electrical angular speeds, electrical angular speed of synchronous flux in the ISM
$F_a$	electromagnetic torque
$\varphi_u, \varphi_v$	$u - v$ axis flux linkages
$P_t$	number of pole
$F_v, F_d, F_{b1}$	electromagnetic torque of the ISM, the output torque of idler 2 and the output torque of the main idler
$f_a, f_c, f_d, f_b$	four moments of inertia in the ISM, in idler 2, in the main idler and in idler 1
$g_v, g_c, g_d, g_b$	four viscid frictional coefficients in the ISM, in idler 2, in the main idler and in idler 1
$\phi_b$	transposition ratios regarding idler 2 and the main idler for the rice milling machine system
$F_b^l(R_{vb}, F_{vb}, F_{vl}, g_b)$	nonlinear coalescence disturbances function
$R_{vb}, F_{vb}, F_{vl}$	rolling force, wind force, braking force
$\mu_v, \mu_b$	speed in idler 2 and the speed in the main idler.
$g_r = g_a + g_c$	coalescence viscid friction coefficient including the main idler and the ISM
$f_r = f_a + f_c$	coalescence moment of inertia including the main idler and the ISM
$\Delta F_a + F_{b1}$	huge comprehensive coalescence disturbances and parameter variations
$F_t(F_{1c}, F_{2c}, F_{3c})$	coalescence torque
$F_{3c}, F_{2c}, F_{1c}$	coulomb friction torque, Stribeck effect torque, adding load torque
$F_{b1}$	comprehensive coalescence disturbances
$\Delta F_a$	comprehensive parameter variations
$\Delta F_a + F_{b1} + F_e$	comprehensive coalescence disturbances
$h_v = -g_r f_r^{-1}$	friendly ratio constant
$R_v(\mu_v)$	bounded with functional-bounded value
$h_w = -f_r^{-1}$	friendly constant concerning the coalescence moment of inertia
$h_x = f_r^{-1}$	friendly constant concerning the coalescence moment of inertia
$R_b, R_c$	two friendly values with bound
$l_v = F_v$	electromagnetic torque of the ISM
$s_a$	speed difference
$c_v$	positive control gain
$l_x, l_y, l_z, l_w$	RRJPNN control, dominator control, two remunerated controls
$a_2^1 = s_a(1 - z^{-1}) = \Delta s_a,$	
$a_1^1 = \mu * -\mu_v = s_a$	speed difference alteration, speed difference
$m, \chi$ and $K$	node number of the center layer, the recurrent gain of the center layer and the iteration number
$\rho_{rt}^1(K), \rho_{ts}^2(K)$	recurrent weight, conjoined weight
$y_r^1, y_s^2, y_t^3$	three linear activation functions in the forehead, center and readward layers

$d_r^1(K), d_s^2(K), d_t^3(K)$	information of three outputs of nodes in the forehead, center and readward layers
$P_s^{(\alpha,\beta)}(b)$	Jacobi polynomial function
$P_0^{(\alpha,\beta)}(b), P_1^{(\alpha,\beta)}(b), P_2^{(\alpha,\beta)}(b)$	0-, 1- and 2-order Jacobi polynomial functions
$d_t^3(K) = l_x$	output information in the readward layer
$D = [d_0^2 \quad \dots \quad d_{m-1}^2]^T$	
$C = [\rho_{10}^2 \quad \dots \quad \rho_{1,m-1}^2]^T$	input information and weight vectors in the readward layer
$\lambda$	minimum difference
$l_x^* = d_t^* = (C^*)^T D$	excellent control rule of the RRJPNN control
$C^*$	excellent weight vector
$\delta$	greater than zero real number
$x_a(t)$	uniformly continuous function
$V_x(0), V_x(t)$	two bounded
$\text{sgn}(\cdot)$	sign function
$V_y$	objective function
$\frac{dC}{dt}$	attunement law
$v_1, v_2$	learning rate of the conjoined weight, learning rate of the recurrent weight
$\tau_1, \tau_2$	two positive evaluation rates
$\hat{\gamma} - \gamma, \hat{\delta} - \delta$	two evaluation differences
$d\hat{\gamma}/dt, d\hat{\delta}/dt$	two evaluation laws
$z_i(n-1), f_i(n-1)$	position of the bat $i$ at $n-1$ time, flight velocity of the bat $i$ at $n-1$ time
$z_i(n), f_i(n)$	position of the bat $i$ at $n$ time, flight velocity of the bat $i$ at $n$ time
$z^*$	current global optimal position
$N_{\max}$	maximum number of iterations
$k_{\max}, k_{\min}$	maximum and minimum frequencies of the soundwaves produced by the bat
$\sigma$	random number at $[-1, 1]$
$z_{old}(n-1)$	solution selected from the current optimal solution at $n-1$ time
$\bar{d}_i(n)$	average loudness from the bat generation at $n$ time
$d_i(n+1), e_i(n+1)$	modified loudness at $n+1$ time, modified pulse rate at $n+1$ time
$e_i(0), d_i(0)$	initial rate, initial loudness
$\zeta, \xi$	constant between 0 and 1, positive constant

## References

- Zuo, L.; Cheng, T.; Zuo, J.; Liu, Y.; Yang, S. A hierarchical intelligent control system for milling machine. In Proceedings of the IEEE International Conference on Intelligent Processing Systems, Beijing, China, 28–31 October 1997; pp. 1–6.
- Huang, S.; Tan, K.K.; Hang, G.S.; Wang, Y.S. Cutting force control of milling machine. *Mechatronics* **2007**, *17*, 533–541. [\[CrossRef\]](#)
- Lobinho, G.; Armando, S. Control of milling machine cutting force using artificial neural networks. In Proceedings of the 6th Iberian Conference on Information Systems and Technologies (CISTI 2011), Chaves, Portugal, 15–18 June 2011; pp. 1–6.
- Tadeusz, M. Numerical control system of conventional milling machine. *Appl. Mech. Mater.* **2016**, *841*, 179–183.
- Tu, F.; Hu, S.; Zhuang, Y.; Lv, J.; Wang, Y.; Sun, Z. Hysteresis curve fitting optimization of magnetic controlled shape memory alloy actuator. *Actuators* **2016**, *5*, 25. [\[CrossRef\]](#)
- Nakshatharan, S.S.; Vunder, V.; Poldsalu, I.; Johanson, U.; Punning, A.; Aabloo, A. Modelling and control of ionic electroactive polymer actuators under varying humidity conditions. *Actuators* **2018**, *7*, 7. [\[CrossRef\]](#)
- Xia, B.; Miriyev, A.; Trujillo, C.; Chen, N.; Cartolano, M.; Vartak, S.; Lipson, H. Improving the actuation speed and multi-cyclic actuation characteristics of silicone/ethanol soft actuators. *Actuators* **2020**, *9*, 62. [\[CrossRef\]](#)
- Lee, T.; Kim, I. Design of a 2DOF ankle exoskeleton with a polycentric structure and a bi-directional tendon-driven actuator controlled using a PID neural network. *Actuators* **2021**, *10*, 9. [\[CrossRef\]](#)
- Wang, L.; Duan, M.; Duan, S. Memristive Chebyshev neural network and its applications in function approximation. *Math. Probl. Eng.* **2013**, *2013*, 1–7. [\[CrossRef\]](#)
- Ting, J.C.; Chen, D.F. Novel mingled reformed recurrent hermite polynomial neural network control system applied in continuously variable transmission system. *J. Mech. Sci. Technol.* **2018**, *32*, 4399–4412. [\[CrossRef\]](#)

11. Soltani, M.; Hegde, C. Fast and provable algorithms for learning two-layer polynomial neural networks. *IEEE Trans. Signal Process.* **2019**, *67*, 3361–3371. [[CrossRef](#)]
12. Ting, J.C.; Chen, D.F. Nonlinear backstepping control of SynRM drive systems using reformed recurrent Hermite polynomial neural networks with adaptive law and error estimated law. *J. Power Electron.* **2018**, *8*, 1380–1397.
13. Richard, A.; James, W. *Some Basic Hypergeometric Orthogonal Polynomials that Generalize Jacobi Polynomials*; American Mathematical Soc.: Providence, RI, USA, 1985; p. 54.
14. Guo, B.Y.; Shen, J.; Wang, L.L. Generalized Jacobi polynomials/functions and their applications. *Appl. Numer. Math.* **2009**, *59*, 1011–1028. [[CrossRef](#)]
15. Rubio, J.J.; Yu, W. Nonlinear system identification with recurrent neural networks and dead-zone Kalman filter algorithm. *Neurocomputing* **2007**, *70*, 2460–2466. [[CrossRef](#)]
16. Chen, D.F.; Shih, Y.C.; Li, S.C.; Chen, C.T.; Ting, J.C. Mixed modified recurring Rogers-Szego polynomials neural network control with mended grey wolf optimization applied in SIM expelling system. *Mathematics* **2020**, *8*, 754. [[CrossRef](#)]
17. Abbasvandi, Z.; Nasrabadi, A.M. A self-organized recurrent neural network for estimating the effective connectivity and its application to EEG data. *Comput. Biol. Med.* **2019**, *110*, 93–107. [[CrossRef](#)]
18. Park, K.; Kim, J.; Lee, J. Visual field prediction using recurrent neural network. *Sci. Rep.* **2019**, *9*, 8385. [[CrossRef](#)]
19. Jaddi, N.S.; Abdullah, S.; Hamdan, A. Multi-population cooperative bat algorithm-based optimization of artificial neural network model. *Inf. Sci.* **2015**, *294*, 628–644. [[CrossRef](#)]
20. Wang, L.; Geng, H.; Liu, P.; Lu, K.; Kolodziej, J.; Ranjan, R.; Zomaya, A.Y. Particle swarm optimization based dictionary learning for remote sensing big data. *Knowl. Based Syst.* **2015**, *79*, 43–50. [[CrossRef](#)]
21. Liu, Z.Z.; Chu, D.H.; Song, C.; Xue, X.; Lu, B.Y. Social learning optimization (SLO) algorithm paradigm and its application in QoS-aware cloud service composition. *Inf. Sci.* **2016**, *326*, 315–333. [[CrossRef](#)]
22. Wu, D.; Xu, S.; Kong, F. Convergence analysis and improvement of the chicken swarm optimization algorithm. *IEEE Access* **2016**, *4*, 9400–9412. [[CrossRef](#)]
23. Gherabia, Y.; Djafri, K.; Krimou, H. Ant colony algorithm for automotive safety integrity level allocation. *Appl. Intell.* **2017**, *8*, 555–569. [[CrossRef](#)]
24. Yang, X.S. A new metaheuristic bat-inspired algorithm. In *Nature Inspired Cooperative Strategies for Optimization (NICSO 2010)*; Springer: Berlin, Heidelberg, 2010; Volume 284, pp. 65–74.
25. Adarsh, B.A.; Raghunathan, T.; Jayabarathi, T.; Yang, X.S. Economic dispatch using chaotic bat algorithm. *Energy* **2016**, *96*, 666–675. [[CrossRef](#)]
26. Wang, Y.; Wang, P.; Zhang, J.; Cui, H.; Cai, X.; Zhang, W.; Chen, J. A novel bat algorithm with multiple strategies coupling for numerical optimization. *Mathematics* **2019**, *7*, 135. [[CrossRef](#)]
27. Chen, D.F.; Cheng, A.B.; Chiu, S.P.C.; Ting, J.C. Electromagnetic torque control for six-phase induction motor expelled continuously variable transmission clumped system using sage dynamic control system. *Int. J. Appl. Electromagn. Mech.* **2021**, *65*, 579–608. [[CrossRef](#)]
28. Singh, G.K.; Nam, K.; Lim, S.K. A simple indirect field oriented control scheme for multiphase induction machine. *IEEE Trans. Ind. Electron.* **2005**, *52*, 1117–1184. [[CrossRef](#)]
29. Guo, Z.; Zhang, J.; Sun, Z.; Zheng, C. Indirect field oriented control of three-phase induction motor based on current-source inverter. *Procedia Eng.* **2017**, *174*, 588–594. [[CrossRef](#)]
30. Han, Y.; Jia, F.; Zeng, Y.; Cao, B. Effects of rotation speed and outlet opening on particle flow in a vertical rice mill. *Powder Technol.* **2016**, *297*, 153–164. [[CrossRef](#)]
31. Zareiforush, H.; Minaee, S.; Alizadeh, M.R.; Samani, B.H. Design, development and performance evaluation of an automatic control system for rice whitening machine based on computer vision and fuzzy logic. *Comput. Electron. Agric.* **2016**, *124*, 14–22. [[CrossRef](#)]
32. Ruekkasaem, L.; Sasananan, M. Optimal parameter design of rice milling machine using design of experiment. *Mater. Sci. Forum* **2018**, *911*, 107–111. [[CrossRef](#)]
33. Astrom, K.J.; Hagglund, T. *PID Controller: Theory, Design, and Tuning*; Instrument Society of America: Research Triangle Park, NC, USA, 1995.
34. Hagglund, T.; Astrom, K.J. Revisiting the Ziegler-Nichols tuning rules for PI control. *Asian J. Control* **2002**, *4*, 364–380. [[CrossRef](#)]
35. Hagglund, T.; Astrom, K.J. Revisiting the Ziegler-Nichols tuning rules for PI control-part II: The frequency response method. *Asian J. Control* **2004**, *6*, 469–482. [[CrossRef](#)]
36. Astrom, K.J.; Wittenmark, B. *Adaptive Control*; Addison-Wesley: New York, NY, USA, 1995.
37. Slotine, J.J.E.; Li, W. *Applied Nonlinear Control*; Prentice-Hall: Englewood Cliffs, NJ, USA, 1991.
38. Chen, D.F.; Shih, Y.C.; Li, S.C.; Chen, C.T.; Ting, J.C. Permanent-magnet SLM drive system using AMRRSPNNB control system with DGWO. *Energies* **2020**, *13*, 2914. [[CrossRef](#)]